

Article

Magnetic Behavior of Carboxylate and β -Diketonate Lanthanide Complexes Containing Stable Organometallic Moieties in the Core-Forming Ligand

Nikolay N. Efimov *, Pavel S. Koroteev *, Andrey V. Gavrikov, Andrey B. Ilyukhin, Zhanna V. Dobrokhotova and Vladimir M. Novotortsev

N.S. Kurnakov Institute of General and Inorganic Chemistry, Russian Academy of Sciences, Leninsky prosp. 31, 119991 Moscow, Russia; penguin1990@yandex.ru (A.V.G.); ilyukhin@igic.ras.ru (A.B.I.); zhdobro@yandex.ru (Z.V.D.); vmnov@igic.ras.ru (V.M.N.)

* Correspondence: nnefimov@narod.ru (N.N.E.); pskoroteev@list.ru (P.S.K.);
Tel.: +7-495-955-48-05 (N.N.E. & P.S.K.)

Academic Editor: Floriana Tuna

Received: 28 July 2016; Accepted: 28 September 2016; Published: 10 October 2016

Abstract: Information concerning the structures of compounds of rare earth elements with carboxylic acids and a β -diketone containing stable organometallic moieties that we obtained previously is presented. Additional results for 15 complexes with the $[Gd_2O_2]$ core allowed confirming and improving the correlation between $J_{Gd-Gd'}$ and the Gd...Gd distance for complexes of this type that we found earlier. For the first time, dc and ac magnetic measurements were carried out for the formerly-described complex $[Dy_2(O_2CCym)_4(NO_3)_2(DMSO)_4]$ (**2**), Cym = $(\eta^5-C_5H_4)Mn(CO)_3$, and two new binuclear complexes, namely $[Dy_2(O_2CFC)_4(NO_3)_2(DMSO)_4]$ (**3**), and $[Dy_2(O_2CFC)_6(DMSO)_2(H_2O)_2]$ (**4**), Fc = $(\eta^5-C_5H_4)Fe(\eta^5-C_5H_5)$. For binuclear $[Dy_2(O_2CCym)_6(DMSO)_4]$ (**1**), as well as for a 1D-polymer $[Dy(O_2CCym)(acac)_2(H_2O)]_n$ (**6**), ac magnetic measurements were carried out more precisely. The characteristics of a single-molecule magnet and of a single-chain magnet were determined for Complexes **2** and **6**, respectively.

Keywords: lanthanide complex; cymantrenecarboxylate; ferrocenecarboxylate; ferrocenoylacetate; magneto-structural correlation; slow magnetic relaxation; molecular magnetism; coordination polymer

1. Introduction

Single-molecule magnets (SMM) are molecule-scale objects that demonstrate properties characteristic of bulk magnetic materials. In compounds of this kind, the classical phenomenon of residual magnetization retention is based on magnetic anisotropy on molecular and atomic levels. The majority of currently-known SMMs are the coordination compounds whose molecules contain a few metal ions with rather a large number of unpaired electrons and can retain residual magnetization for some time at very low temperatures. Compounds of this kind may be regarded as elements of high-density magnetic memory, i.e., promising components for data storage. A powerful impetus to the developments in this field was given by studies of the magnetic properties of the $\{Mn_{12}\}$ cluster [1,2]. Currently, close attention of researchers is given to coordination compounds of lanthanides in the context of molecular magnetism.

The interest in coordination compounds of rare earth elements (REE) is currently rather high [3,4], primarily due to their unique magnetic properties [5–9]. Among them, considerable attention is paid to β -diketonate and carboxylate derivatives. The latter class of compounds is characterized by a wide structural variety that is mainly reached due to the ability of carboxylic groups to show various structural functions. It is also attained by incorporation of additional ligands [10]. The most

popular approach to the design of lanthanide-containing SMM involves the use of ligand field symmetry to increase the anisotropy of isolated Ln^{3+} ions [11]. At the same time, beside the specifics of the local symmetry of Dy^{3+} , a considerable role may belong to the ligand nature (electrostatic aspect) [12]. Therefore, the suggestion of new core-forming ligands for directed design of SMM is of undoubted interest.

An interesting, but insufficiently studied group among carboxylate and β -diketonate lanthanide derivatives comprises complexes in which the core-forming (carboxylate/ β -diketone) ligand contains stable organometallic moieties, viz. derivatives of ferrocene (bis(η^5 -cyclopentadienyl)iron, (η^5 -C₅H₅)₂Fe), and cymantrene (η^5 -cyclopentadienyltricarbonylmanganese, (η^5 -C₅H₅)Mn(CO)₃), the derivatives of cymantrene- and ferrocene-carboxylic acids in particular (Scheme 1).



Scheme 1. (a) cymantrenecarboxylic acid (CymCO₂H); (b) ferrocenecarboxylic acid (FcCO₂H).

These ligands are bulky; they also have a highly polarizable π -system. Therefore, both steric and electronic effects may play a significant role in metal carboxylates/ β -diketonates. Such compounds also represent the original type of heterometallic complexes, since they are potentially able to combine specific properties of the metal ion and of the organometallic fragment. For example, in the aspect of magnetic properties, the reversible conversion of the ferrocenyl group to paramagnetic ferrocenium in the solid state of ferrocenecarboxylates is of interest [13,14].

This paper provides a review of our previous (2011–2016) and new synthetic and structural results of studies on the magnetic behavior of cymantrene- and ferrocene-carboxylates of dysprosium.

2. Results and Discussion

First of all, no information about cymantrenecarboxylates of rare earth metals and their magnetic properties was available before our first publication [15]. To date, we have obtained cymantrenecarboxylates with various structures, both binuclear [15–18] and polymeric complexes [19–21].

The first complexes of this type that we obtained included two similar series of heteroleptic cymantrenecarboxylates of light lanthanides, $[Ln_2(\mu-O, \eta^2-O_2CCym)_2(\mu_2-O, O'-O_2CCym)_2(\eta^2-O_2CCym)_2(L)_4] nL$, containing molecules of volatile tetrahydrofuran ($Ln = Nd, n = 0; Ln = Gd, Eu, n = 1; L = THF$) [15] or pyridine ($Ln = Pr, Sm, Eu, Gd, n = 2, L = Py$) [16] as neutral ligands. The obtained complexes had a binuclear structure typical of lanthanide carboxylates (Figure 1).

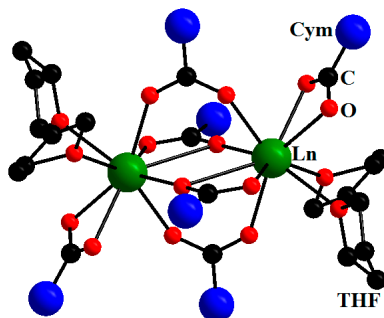


Figure 1. Molecular structure of $[Ln_2(\mu-O, \eta^2-O_2CCym)_2(\mu_2-O, O'-O_2CCym)_2(\eta^2-O_2CCym)_2(THF)_4]$. Reproduced from the work [15] with the change in appearance.

Furthermore, a series of binuclear complexes that contained relatively low volatile DMSO as the neutral ligand was obtained, namely $[Ln_2(\mu\text{-O},\eta^2\text{-O}_2\text{CCym})_2(\mu\text{-O},\text{O}'\text{-O}_2\text{CCym})_2(\eta^2\text{-O}_2\text{CCym})_2(\text{DMSO})_4]$; $Ln = \text{Ce}, \text{Nd}, \text{Eu}, \text{Gd}$ [17]; $Ln = \text{Tb}, \text{Dy}$ [18].

The first representatives of lanthanide cymantrenecarboxylates with the ratio $Ln:Mn = 1:2$ were binuclear compounds $[Ln_2(\mu\text{-O}_2\text{CCym})_2(\mu\text{-O},\eta^2\text{-O}_2\text{CCym})_2(\eta^2\text{-NO}_3)_2(\eta^2\text{-DME})_2]$ ($Ln = \text{Pr}, \text{Eu}, \text{Gd}, \text{Tb}, \text{Dy}, \text{Ho}, \text{Er}$; DME (1,2-dimethoxyethane)) [19] and $[Ln_2(\mu\text{-O},\text{O}'\text{-O}_2\text{CCym})_4(\eta^2\text{-NO}_3)_2(\text{DMSO})_4]$ ($Ln = \text{Tb}, \text{Dy}$) [18]. The $[Ln_2(\text{O}_2\text{CCym})_4(\text{NO}_3)_2(\text{DME})_2]$ complexes are built similarly to binuclear complexes with THF, pyridine and DMSO, except that the role of chelating anions is played by nitrate ions, whereas chelate molecules of DME are the neutral ligands. Yet another type of compound with the $Ln:Mn$ ratio of 1:2 is the mixed acetate-cymantrenecarboxylate complexes [20]. In the case of heavier lanthanides (Ho, Er, Tm), binuclear complexes $[Ln_2(\mu\text{-O}_2\text{CCym})_2(\eta^2\text{-O}_2\text{CCym})_2(\eta^2\text{-OAc})_2(\text{H}_2\text{O})_4]\cdot 5\text{H}_2\text{O}$ were obtained (Figure 2), while 1D polymers $[Ln(\text{O}_2\text{CCym})_2(\text{OAc})(A)_x]_n\cdot m\text{Solv}$ ($x = 1, 2$; $A = \text{MeOH}, \text{H}_2\text{O}$; $\text{Solv} = i\text{-PrOH}, \text{THF}, \text{H}_2\text{O}$) were obtained in the cases of $Ln = \text{Nd}, \text{Gd}, \text{Dy}$ (Figure 3) [20].

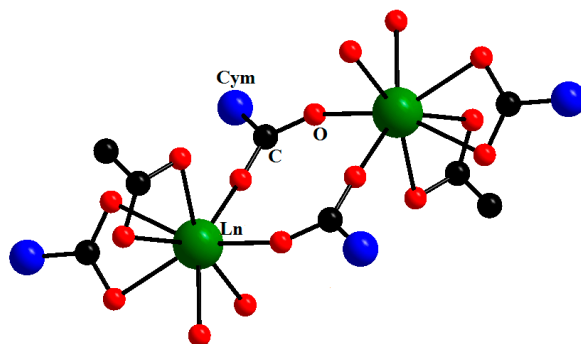


Figure 2. Molecular structure of $[Ln_2(\mu\text{-O}_2\text{CCym})_4(\text{OAc})_2(\text{H}_2\text{O})_4]\cdot 5\text{H}_2\text{O}$ ($Ln = \text{Ho}, \text{Er}, \text{Tm}$). Reproduced from the work [20] with the change in appearance.

All of the polymers include a common ladder structure $\{Ln(\text{OAc})\}_n$ formed by tetradentate acetate ligands and Ln^{3+} ions. Cymantrenecarboxylate anions form the periphery of the polymer chain, where they play the role of monodentate, chelate or bridging ligands. The diversity of coordinating functions of the cymantrenecarboxylate residues determines the variety of the polymer structures.

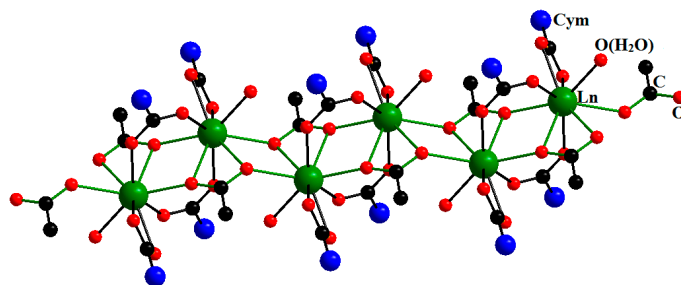


Figure 3. Molecular structure of $[Ln(\text{O}_2\text{CCym})_2(\text{OAc})(A)_x]_n\cdot m\text{Solv}$ ($Ln = \text{Nd}, \text{Gd}, \text{Dy}$; $x = 1, 2$; $A = \text{MeOH}, \text{H}_2\text{O}$; $\text{Solv} = i\text{-PrOH}, \text{THF}, \text{H}_2\text{O}$). Reproduced from the work [20] with the change in appearance.

The 1D-polymeric complexes $[Ln(\eta^2\text{-O}_2\text{CCym})_2(\mu\text{-O}_2\text{CCym})_4Ln(\text{ROH})_4]_n\cdot m\text{Solv}$ ($Ln = \text{Nd}, \text{Gd}, \text{Dy}, \text{Ho}, \text{Er}$; $R = \text{H}, \text{Me}$; $\text{Cym} = (\eta^5\text{-C}_5\text{H}_4)\text{Mn}(\text{CO})_3$; Solv (solvent molecule)) that we obtained appeared to be rather interesting. The polymeric chains of these compounds contain two types of alternating coordination centers, namely, Ln^{3+} ions that coordinate the water/methanol molecules and the oxygen atoms of bridging carboxylate anions and Ln^{3+} ions that coordinate the oxygen atoms of

bridging and chelate carboxylate anions; in both cases, the coordination number (CN) of Ln equals eight (Figure 4) [21].

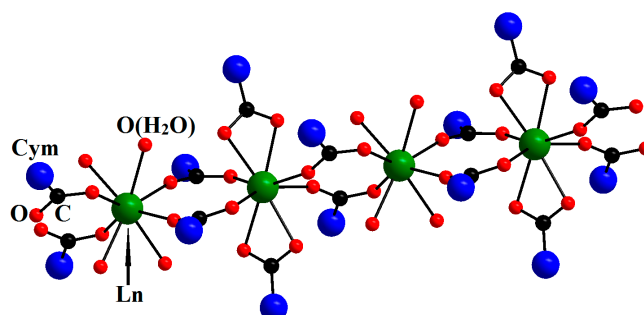


Figure 4. Molecular structure of $[Ln(\eta^2\text{-O}_2\text{CCym})_2(\mu\text{-O}_2\text{CCym})_4Ln(\text{H}_2\text{O})_4]_n$. Reproduced from the work [21] with the change in appearance.

To synthesize cymantrenecarboxylates with the ratio $Ln:Mn = 1:1$, we suggested an original technique with the use of hydrated lanthanide acetylacetonates as the starting reagents [22]. 1D-polymeric complexes $[Ln(\text{O}_2\text{CCym})(\text{acac})_2(\text{H}_2\text{O})]_n$ ($Ln = \text{Eu, Gd, Tb, Dy, Ho, Er}$) were obtained. The structure of the complexes is formed of $[Ln(\text{acac})_2(\text{H}_2\text{O})]$ moieties, in which the lanthanide ion is chelated by two acac ligands, while the bridging cymantrenecarboxylate anions bind the adjacent $[Ln(\text{acac})_2(\text{H}_2\text{O})]$ moieties into an infinite chain. The coordination number of Ln^{3+} is seven, which is a comparatively small value for lanthanide complexes (Figure 5).

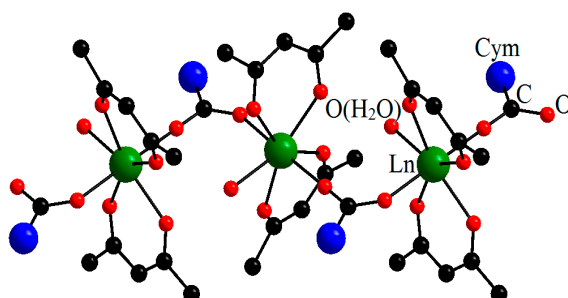


Figure 5. Molecular structure of $[Ln(\text{O}_2\text{CCym})(\text{acac})_2(\text{H}_2\text{O})]_n$ ($Ln = \text{Eu–Er}$). Reproduced from the work [22] with the change in appearance.

Moreover, new REE ferrocenecarboxylates $[Ln_2(\mu\text{-O},\eta^2\text{-OOCFc})_2(\mu_2\text{-O},\text{O}'\text{-OOCFc})_2(\eta^2\text{-NO}_3)_2(\text{DMSO})_4]$ ($Ln = \text{Gd, Tb, Y}$) and $[\text{Gd}_2(\mu\text{-O},\eta^2\text{-OOCFc})_2(\eta^2\text{-OOCFc})_4(\text{DMSO})_2(\text{H}_2\text{O})_2] \cdot 2\text{DMSO} \cdot 2\text{CH}_2\text{Cl}_2$ were obtained and characterized [23]. Two new compounds were obtained in this study: $[\text{Dy}_2(\text{O}_2\text{CFc})_4(\text{NO}_3)_2(\text{DMSO})_4]$ (**3**), which is isostructural with $[Ln_2(\text{O}_2\text{CFc})_4(\text{NO}_3)_2(\text{DMSO})_4]$ ($Ln = \text{Gd, Tb, Y}$) [23], and $[\text{Dy}_2(\text{O}_2\text{CFc})_6(\text{DMSO})_2(\text{H}_2\text{O})_2] \cdot 2\text{DMSO} \cdot 3\text{MePh}$ (**4**).

A number of hitherto unknown ferrocenoylacetate complexes of rare earth elements, $[Ln(\text{fca})_3(\text{bpy})] \cdot \text{MeC}_6\text{H}_5$ ($Ln = \text{Pr, Eu, Gd, Tb, Dy, Ho}$ ($\text{fca} = \text{Fc}(\text{CO})\text{CH}(\text{CO})\text{Me}$; $\text{bpy} = 2,2'$ -bipyridyl)) (Figure 6) [24] and $[Ln(\text{fca})_2(\text{NO}_3)(\text{bpy})] \cdot n\text{MeC}_6\text{H}_5$ ($Ln = \text{Sm, Eu, Dy, Er, Yb}$), were synthesized and characterized by X-ray single crystal analysis [25].

Thus, we proposed methods for the synthesis of new compounds, determined their molecular and crystal structures, studied their thermal behavior, as well as luminescent properties for Eu derivatives [15–25], but a detailed study of the magnetic behavior of some of the complexes was not carried out.

The diamagnetism of cymantrene and ferrocene moieties distinguishes lanthanide cymantrene- and ferrocene-carboxylates from all of the other Fe- Ln and Mn- Ln heterometallic compounds since their

magnetism is caused only by the contribution of Ln^{3+} ions. The dc magnetic susceptibility for most of the complexes was studied in the temperature range of 2–300 K in an applied magnetic field of 5000 Oe. It was shown that their magnetic behavior was determined by the lanthanide ions, and the χT (300 K) values for all of the compounds agreed satisfactorily with the theoretical values [26].

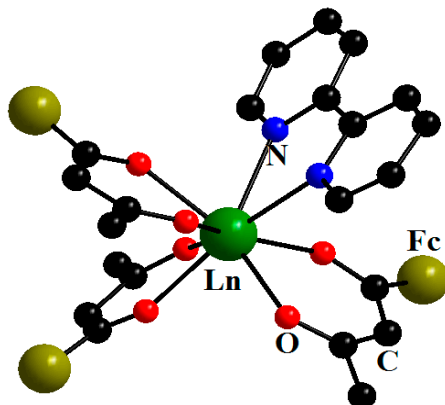


Figure 6. Molecular structure of $[Ln(fca)_3(bpy)]$ ($Ln = Pr, Eu, Gd, Tb, Dy, Ho$); here and below, the ferrocene moieties are simplified for clarity. Reproduced from the work [24] with the change in appearance.

Among compounds of light lanthanides (Ce–Gd), complexes of Gd^{3+} are of particular interest due to the electronic structure of this ion: it has the maximum possible number of unpaired electrons ($S = 7/2$) among 4f-elements. Moreover, it is an isotropic ion with zero contribution from spin-orbital coupling, which considerably facilitates the mathematical description of magnetism for Gd^{3+} complexes. The experimental $\chi_m T(T)$ dependences for binuclear and polynuclear Gd^{3+} complexes with the $[Gd_2O_2]$ core are usually interpreted using equations derived from the Heisenberg–Dirac–Van Vleck Hamiltonian $H = -JS_{Gd}S_{Gd'}$ (J : exchange coupling constant) with isotropic spin and the quantum number $S_{Gd} = S_{Gd'} = 7/2$ [27,28].

For binuclear Gd^{3+} complexes both ferromagnetic and antiferromagnetic interactions with small absolute values J have been observed (below 0.2 cm^{-1}). The ferromagnetic nature of the $Gd \dots Gd$ interaction was supported by magnetization measurements in the 0–5 T range at 2 K [29]. Relative expanded uncertainties $U_r(J)$ are not presented in the literature (see the references in the work [30] and in Table 1). The fitting procedure leads to $J_{ex, g}$ and ($R = \Sigma[(\chi_m)_{obs} - (\chi_m)_{calc}]^2 / \Sigma[(\chi_m)_{obs}]^2$), which allows one to evaluate $U_r(J)$. $U_r(J)$ must be not less than 10% (± 0.01).

The problem of establishing the magnetostructural correlation for gadolinium complexes with the $[Gd_2O_2]$ core has been considered earlier [31–33]. The experimental data that we obtained for $[Gd_2(O_2CCym)_6(THF)_4] \cdot THF$ [15] and $[Gd_2(O_2CCym)_6(py)_4] \cdot 2py$ [16] and the available sufficiently abundant data for 34 gadolinium complexes with the $[Gd_2O_2]$ motive allowed us to suggest a correlation between the $J_{Gd-Gd'}$ value and the $Gd \dots Gd$ distance in the complexes [30]. The determined empirical dependence was satisfactorily approximated by a fourth degree polynomial with $R^2 = 0.854$ [30]. It was found that the antiferromagnetic interaction between the Gd^{3+} ions weakens with an increase in the distance; at $D_{Gd \dots Gd'}$ above $\sim 4.10 \text{ \AA}$, it changes to ferromagnetic coupling that passes through a maximum (at $D_{Gd \dots Gd'} \approx 4.25 \text{ \AA}$) and approaches zero at $D_{Gd \dots Gd'} > 4.50 \text{ \AA}$ (Figure 7). The authors [34] also note that within the framework of the $[Gd_2O_2]$ core, exchange coupling is ferromagnetic when the $Gd \dots Gd$ distance is larger than ~ 4.0 – 4.1 \AA , while the exchange coupling is antiferromagnetic when this parameter is smaller.

The validity of this correlation was confirmed by the data for four $[Gd_2O_2]$ complexes synthesized by us (marked with asterisks in Table 1 and by blue points in Figure 7) [30]. The plot of the dependence is similar to the Bethe–Slater curve (Figure 7, insert) which represents the magnitude of direct exchange

as a function of a/r ratio, where a is the distance between two nearby atoms, and r is the radius of the unfilled electron shell [35].

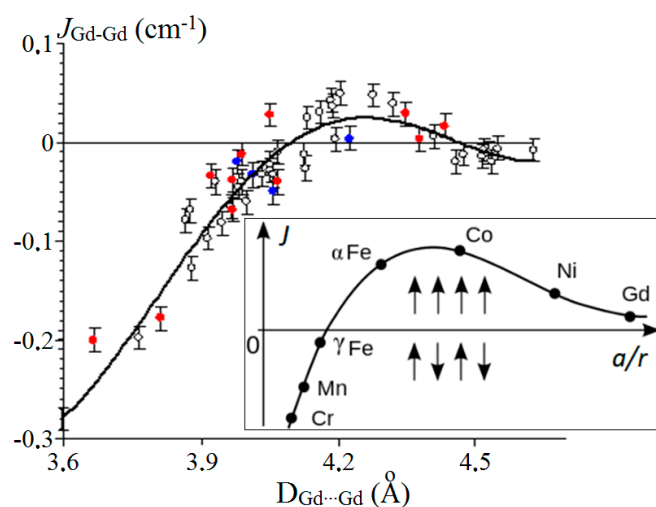


Figure 7. Approximation of the dependence of $J_{\text{Gd-Gd}'}$ vs. Gd...Gd' distance for 49 $[\text{Gd}_2\text{O}_2]$ complexes (o, values used for building of the plot in the work [30]; ●, values reported in the work [30], but not used for building of the correlation; ●, newly-added data (Table 1)). The relative expanded uncertainties are shown. Insert: Bethe–Slater curve [35].

In the work [30], the results of the studies carried out before the year 2013 were summarized. However, presently, this problem is still under research [34]. Therefore, we decided to supplement the information provided in our earlier work [30] with both our and literature data, which is presented in this paper (Table 1 and red points in Figure 7).

Table 1. The Gd...Gd' distances and the exchange coupling parameter $J_{\text{Gd-Gd}'}$ for $[\text{Gd}_2\text{O}_2]$ complexes.

Compound	$D_{\text{Gd}\dots\text{Gd}'}$, Å	$J_{\text{Gd-Gd}'}$, cm^{-1}	Reference
$[\text{Gd}_2(\text{H}_2\text{L})_2(\text{piv})_4] \cdot 2\text{CHCl}_3$	3.665	−0.19	[36]
$[\text{Gd}_2(\text{valdien})_2(\text{NO}_3)_2]$	3.811	−0.178	[37]
$[\text{Gd}_2(\text{O}_2\text{CMe})_4(\text{H}_2\text{L}^1)_2](\text{ClO}_4)_2 \cdot 2\text{H}_2\text{O} \cdot 2\text{MeOH}$	3.920	−0.033	[34]
$[\text{Gd}(\text{O}_2\text{CCym})_2(\text{OAc})(\text{H}_2\text{O})_2]_n \cdot 2n\text{H}_2\text{O}$	3.968	−0.038	[20]
$[\text{Gd}_2(\text{O}_2\text{CCym})_4(\text{NO}_3)_2(\text{DME})_2]$	3.970	−0.068	[19]
$[\text{Gd}_2(\text{Piv})_6(\text{phen})_2]^*$	3.978	−0.020	[30]
$[(\text{CO}_3)_2\{\text{Ni}(3\text{-MeOsaltN})(\text{MeOH})\text{Gd}(\text{NO}_3)_2\}]$	3.989	−0.012	[38]
$[\text{Gd}_2(\text{Piv})_6(\text{bipy})_2]^*$	4.014	−0.033	[30]
$[(\text{CO}_3)_2\{\text{ZnL}^2\text{Gd}(\text{NO}_3)_2\}]$	4.050	0.028	[39]
$[\text{Gd}_2(\text{O}_2\text{CCym})_6(\text{DMSO})_4]^*$	4.058	−0.050	[30]
$[\text{Gd}_2(\text{O}_2\text{CFc})_4(\text{NO}_3)_2(\text{DMSO})_4]$	4.067	−0.040	[23]
$[\text{Gd}_2(\text{Piv})_6(\text{bath})_2]^*$	4.224	0.004	[30]
$[\text{Gd}_2(\text{O}_2\text{CFc})_6(\text{DMSO})_2(\text{H}_2\text{O})_2] \cdot 2\text{DMSO} \cdot 2\text{CH}_2\text{Cl}_2$	4.348	0.029	[23]
$[\text{Gd}_2(\text{O}_2\text{CC}_6\text{H}_3(\text{NO}_2)_2)_6(\text{DMSO})_4] \cdot 3\text{MePh}$	4.380	0.003	[40]
$[\text{Gd}_2(\text{O}_2\text{CC}_6\text{H}_3(\text{NO}_2)_2)_6(\text{DMSO})_4] \cdot 3(\text{Me}_2\text{N})\text{C}_6\text{H}_5$	4.435	0.017	[40]

* The complexes used for correlation test in the work [27]; H_3L = 2,2'-(2-hydroxy-3-methoxy-5-methylbenzylazanediyl)diethanol; Hpiv = pivalic acid; $\text{H}_2\text{valdien}$ = $N1,N3$ -bis(3-methoxysalicylidene) diethylenetriamine; H_2L^1 = bis(5-methylimidazol-4-yl-methylideneaminopropyl)methylamine; phen = 1,10-phenanthroline; 3-MeOsaltN = N,N' -bis(3-methoxy-2-oxybenzylidene)-1,3-propanediaminato; bipy = 2,2'-bipyridyl; L^2 = N,N' -bis(3-methoxy-2-oxybenzylidene)-1,3-propanediaminato; bath = bathophenanthroline.

Taking into account additional findings, together with the previously used data, allowed enhancing the reliability of the correlation ($R^2 = 0.875$). As can be seen from Figure 7, these data also confirm the validity of the correlation that we found.

It should be noted that small negative J values are observed in the area of long Gd...Gd distances (Figure 7). This may be due to the influence of factors other than Gd...Gd distance, which we have neglected. However, the relative expanded uncertainty suggests that small positive J values are also possible in this region. The J values corresponding to the longest Gd...Gd distances are very close to zero, as expected.

Furthermore, the following dysprosium compounds were studied: $[\text{Dy}_2(\text{O}_2\text{CCym})_6(\text{DMSO})_4]$ (1), $[\text{Dy}_2(\text{O}_2\text{CCym})_4(\text{NO}_3)_2(\text{DMSO})_4]$ (2), $[\text{Dy}_2(\text{O}_2\text{CFc})_4(\text{NO}_3)_2(\text{DMSO})_4]$ (3), $[\text{Dy}_2(\text{O}_2\text{CFc})_6(\text{DMSO})_2(\text{H}_2\text{O})_2] \cdot 2\text{DMSO} \cdot 3\text{MePh}$ (4), $[\text{Dy}(\eta^2\text{-O}_2\text{CCym})_2(\mu\text{-O}_2\text{CCym})_4\text{Dy}(\text{H}_2\text{O})_4]_n$ (5), $[\text{Dy}(\text{O}_2\text{CCym})(\text{acac})_2(\text{H}_2\text{O})]_n$ (6) and $[\text{Dy}(\text{fca})_3(\text{bpy})] \cdot \text{MeC}_6\text{H}_5$ (7).

Binuclear cymantrenecarboxylates 1 were 2 were prepared and structurally characterized earlier [18]; dysprosium ferrocenecarboxylates 3 and 4 are newly obtained.

The cymantrenecarboxylate anion is the core-forming ligand in Compounds 1 and 2, whereas the ferrocenecarboxylate anion plays this role in Structures 3 and 4. Structures 1, 2, 3 and 4 are formed by centrosymmetric dimers (Figure 8).

The coordination number of Dy atoms in Structure 1 is nine. The coordination polyhedron is best described as a three-cap trigonal prism. The structure of the dimer of Compound 2 is similar to the structure of Compound 1 with the replacement of chelate ligands, i.e., the $\{\eta^2\text{-O}_2\text{CCym}\}$ ligand, for $\{\eta^2\text{-NO}_3\}$. Furthermore, on transition from Compounds 1 to 2, the chelate-bridging $\{\mu\text{-O}, \eta^2\text{-O}_2\text{CCym}\}$ cymantrenecarboxylate ligands turn in such a way that they become purely bridging $\{\mu_2\text{-O}, \text{O}'\text{-O}_2\text{CCym}\}$ ligands, which results in a decrease in the CN from nine (1) down to eight (2) and a considerable increase in the Dy...Dy' distance from 4.0513(6)–4.1775(4) Å, respectively. In Structure 3, two Dy atoms are bound by two bridging and two chelate-bridging O_2CFc ligands, similarly to Structure 1. Coordination of Dy is also complemented by a NO_3^- chelate ion and two oxygen atoms of DMSO molecules (CN = 9); the Dy...Dy' distance is 4.042 Å. In Structure 4, two Dy atoms are bound by two O_2CFc bridging ligands; coordination of Dy is complemented by two O_2CFc chelate ligands and two oxygen atoms from molecules of DMSO and water (CN = 8); the Dy...Dy' distance is 4.376 Å.

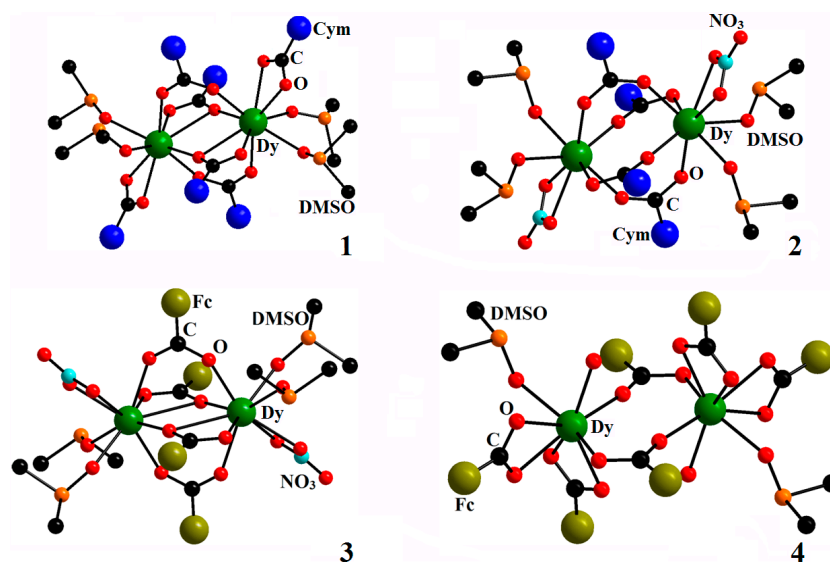


Figure 8. Molecular structures of Compounds 1 [18] (reproduced with the change in appearance), 2 [18] (reproduced with the change in appearance), 3 and 4.

DC magnetic measurements were carried out for Complexes 2, 3 and 4 for the first time. The $\chi_m T$ values of complexes at 300 K (Table 2) correspond to two magnetically-isolated free Dy^{3+} ions (${}^6\text{H}_{15/2}$, $S = 5/2$, $L = 5$, $g = 4/3$).

Table 2. Magnetic characteristics of Complexes 1–4.

Complex	$\chi_m T$ (300 K) $\text{cm}^3 \cdot \text{mol}^{-1} \cdot \text{K}$	$\chi_m T$ (theor) $\text{cm}^3 \cdot \text{mol}^{-1} \cdot \text{K}$ [26]	$\chi_m T$ (2 K) $\text{cm}^3 \cdot \text{mol}^{-1} \cdot \text{K}$
$[\text{Dy}_2(\text{O}_2\text{CCym})_6(\text{DMSO})_4]$ (1)	28.71 [18]		20.10
$[\text{Dy}_2(\text{O}_2\text{CCym})_4(\text{NO}_3)_2(\text{DMSO})_4]$ (2)	28.67	28.34	18.31
$[\text{Dy}_2(\text{O}_2\text{CFc})_4(\text{NO}_3)_2(\text{DMSO})_4]$ (3)	28.37		15.21
$[\text{Dy}_2(\text{O}_2\text{CFc})_6(\text{DMSO})_2(\text{H}_2\text{O})_2]$ (4)	28.77		14.88

As the temperature decreases to 100 K, the $\chi_m T$ values of dysprosium complexes weakly depend on temperature, but on further temperature lowering, the absolute values decrease considerably. The minimum values are attained at 2 K (Figure S1, Table 2). This behavior is caused by the splitting of m_J levels in the zero field due to the ligand field effect, by the Zeeman effect under the external field and/or by weak antiferromagnetic coupling between the lanthanide ions.

To explore the presence of the slow relaxation of magnetization in the case of Dy complexes, dynamic measurements of ac magnetic susceptibility as a function of temperature at variable frequencies were performed for polycrystalline powder samples of some complexes in the temperature range of 2–12 K. Such measurements for Complexes 2–4 were also carried out for the first time.

For binuclear complex $[\text{Dy}_2(\text{O}_2\text{CCym})_6(\text{DMSO})_4]$ (1), we have measured the ac magnetic susceptibility in the dc field with the intensities $H = 0$ and 5 kOe only for three frequencies earlier [18]. In the zero external field, the temperature dependences of the imaginary component contain the frequency-dependent signal and a noticeable increase in χ'' , but no distinctly detected maximum was observed. As the field intensity increases to $H = 5$ kOe, the maximum in the $\chi''(T)$ dependences is observed in the range 4.5–5 K at all frequencies (only three frequencies (100 Hz, 1 kHz and 10 kHz)) at which the measurements were carried out [18].

In this work, Complex 1 was studied in the temperature range of 2–5 K in zero, 1000 and 2000 Oe external fields for a wide range of frequencies (10–10,000 Hz). A frequency-dependent signal χ'' is observed in this temperature range, but the position of the maximum in the $\chi''(\nu)$ plot does not change with the temperature variation (Figure S2), which may be due to the quantum tunneling effect. On application of the magnetic field with up to an $H = 2000$ Oe strength, the maximum in the $\chi''(T)$ plot is observed at all of the measurement temperatures, but no shift of the maximum is observed (Figure S3). This behavior of the $\chi''(\nu)$ plot indicates that slow magnetic relaxation is present, but the effect of quantum tunneling decreases insignificantly upon the application of an external magnetic field.

Furthermore, we carried out studies for binuclear complex $[\text{Dy}_2(\text{O}_2\text{CCym})_4(\text{NO}_3)_2(\text{DMSO})_4]$ (2). For Complex 2, non-zero χ'' values are observed even in the zero field (Figure 9).

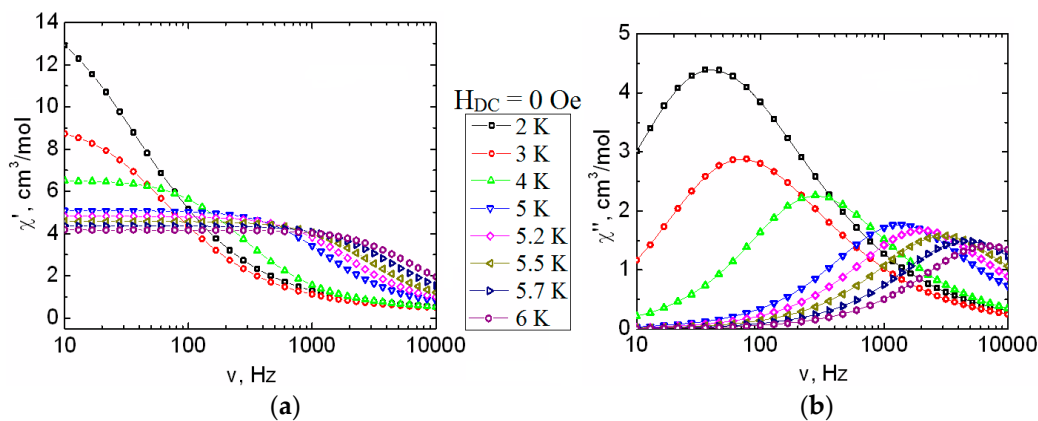


Figure 9. Frequency dependence of the in-phase (χ' , a) and out-of-phase (χ'' , b) parts of ac susceptibility, between 2 and 6 K, for 2 in the zero dc field. Solid lines are visual guides.

The τ vs. T^{-1} plot for Complex **2** is presented in Figure S4 and Figure 10 (empty squares). Fitting the $\tau(T^{-1})$ plot to the Arrhenius equation in the temperature range of 2–6 K allowed us to determine the potential barrier of magnetization reversal, $\Delta E/k_B = 53$ K, and the pre-exponential factor, $\tau_0 = 3.2 \cdot 10^{-9}$ s.

The magnetization dynamics of **2** was also studied under an applied dc magnetic field in order to minimize the probability of quantum tunneling (Figure S5). It was found that the external magnetic field did not affect considerably the relaxation processes in Complex **2** (Figure 10).

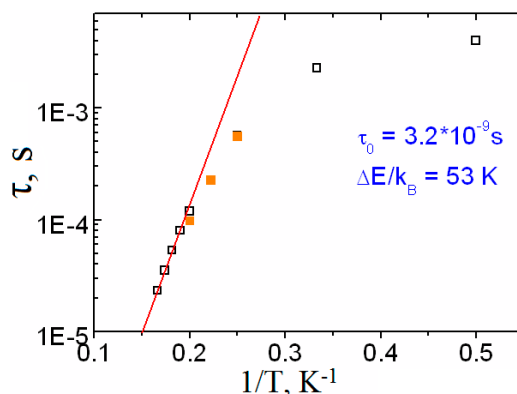


Figure 10. τ vs. T^{-1} plot for $[\text{Dy}_2(\text{O}_2\text{CCym})_4(\text{NO}_3)_2(\text{DMSO})_4]$ (**2**) in a zero (\square) and 1000 Oe (\blacksquare) dc field. The solid red line is the best fit to the Arrhenius law ($\tau_0 = 3.2 \times 10^{-9}$ s, $\Delta E/k_B = 53$ K) (this study).

No non-zero out-of-phase component of ac magnetic susceptibility χ'' was found for Complex **3** at temperatures above 2 K in the frequency range of 10–10,000 Hz, both in the zero magnetic field and under an external magnetic field of 5000 Oe (Figures S6–S8).

In the case of the new complex $[\text{Dy}_2(\text{O}_2\text{CFC})_6(\text{DMSO})_2(\text{H}_2\text{O})_2]$ (**4**), a frequency-dependent signal χ'' is almost not observed in the zero external field at 2 K. On increasing the dc field strength to $H = 2500$ Oe, a $\chi''(\nu)$ growth is observed at all magnetic field strengths applied for the measurements, but no maximum was found on the $\chi''(\nu)$ plots (Figure S9).

The study of binuclear Complexes **1–4** that we performed has shown that Complex **2** has the best SMM characteristics, whereas no SMM properties were found in Complex **3**. Interestingly, the lowering of the coordination number in the corresponding pairs **1** and **2**, and **3** and **4** takes place. The results obtained agree with the concept that changes in local molecular symmetry and even insignificant distortion of coordination geometry [41], as well as possible dipole coupling of Dy(III) ions [42] have a considerable effect on SMM characteristics. The enhancement of SMM properties with the lowering of the coordination number observed in our case is in agreement with the recent theoretical study [43].

Studies of polymeric complex $[\text{Dy}(\eta^2\text{-O}_2\text{CCym})_2(\mu\text{-O}_2\text{CCym})_4\text{Dy}(\text{H}_2\text{O})_4]_n$ (**5**) (whose molecular structure is shown in Figure 4) were performed previously [21]. Maxima were observed in the zero field on the frequency dependences of out-of-phase component χ'' at low temperatures (2–3 K), which confirms the presence of slow relaxation of the magnetization (Figure S10). Analysis of the isotherms of frequency dependences gave the relaxation time. Figure S11 shows the dependence of relaxation time on inverse temperature in the temperature range of 2.0–3.5 K. Using the Arrhenius law $\tau = \tau_0 \cdot \exp(\Delta E/k_B T)$, the pre-exponential factor ($\tau_0 = 4.3 \times 10^{-6}$ s) and the relaxation energy barrier ($\Delta E/k_B = 4.1$ K) were determined. The shape of $\ln(\tau)$ vs. $(1/T)$ and $\chi''(\chi')$ plots (Figure S12) allow us to believe that relaxation is thermally activated and that a purely quantum mode takes place below the temperature studied ($T < 2$ K). A unit of the polymeric chain $[\text{Dy}(\eta^2\text{-O}_2\text{CCym})_2(\mu\text{-O}_2\text{CCym})_4\text{Dy}(\text{H}_2\text{O})_4]_n$ (**5**) contains two Dy atoms, one of which coordinates four O atoms of $\{\mu\text{-O}_2\text{CCym}\}$ ligands and four O atoms of H_2O molecules (Figure 4). The second Dy atom coordinates four O atoms of $\{\mu\text{-O}_2\text{CCym}\}$ and four O atoms of $\{\eta^2\text{-O}_2\text{CCym}\}$ ligands. The coordination number of Dy atoms is eight; the $\{\text{Dy}(\mu\text{-O}_2\text{CCym})_4(\text{H}_2\text{O})_4\}$ polyhedron is

a two-cap trigonal prism. The $\{\text{Dy}(\eta^2\text{-O}_2\text{CCym})_2(\mu\text{-O}_2\text{CCym})_4\}$ polyhedron is strongly distorted and is most similar to a trigonal dodecahedron with the central segments of the trapezohedra occupied by $\eta^2\text{-O}_2\text{C}$ moieties. It has been shown [44] that the existence of magnetic centers with differing anisotropy can give rise to two different mechanisms of magnetic relaxation that correspond to two different positions of dysprosium atoms. Though Structure 5 contains two crystallographically different Dy centers, studies have shown that only one mechanism of thermally-activated magnetic relaxation is present.

The structure of a polymeric complex $[\text{Dy}(\text{O}_2\text{CCym})(\text{acac})_2(\text{H}_2\text{O})]_n$ (6) is formed by polymeric chains (Figure 5); the coordination number of Dy is seven; the polyhedron is a pentagonal bipyramid. Previously, incomplete study of this complex was carried out [21]. The temperature dependences of the out-of-phase alternating-current (ac) magnetic susceptibility in the zero external magnetic field were obtained. However, no application of an external magnetic field was made. In this study, the dynamics of the magnetization was probed by ac susceptibility measurements for Complex 6. At 2 K, an ac relaxation mode for 6 appears around 2000 Oe. From the complete study of the ac susceptibility as a function of temperature and frequency at 2000 Oe (Figure 11), the characteristic relaxation time of the magnetization was estimated between 2 and 10 K (Figure S15). As shown by the non-thermally-activated dependence of the relaxation time in this temperature range, quantum tunneling of the magnetization is obviously dominating the relaxation process in 6 even under the applied dc field. Nevertheless, an attempt to extrapolate the Arrhenius behavior above 10 K leads to a rough estimation of the SMM energy gap of about 42 K, with a pre-exponential factor of 4.3×10^{-7} s. The value of τ_0 , which is at least four orders of magnitude larger than expected for typical vibrations of the network, further confirms that the estimation value of $\Delta E/k_B$ should be considered as a lower limit of the actual energy barrier for the thermally-activated relaxation process in 6.

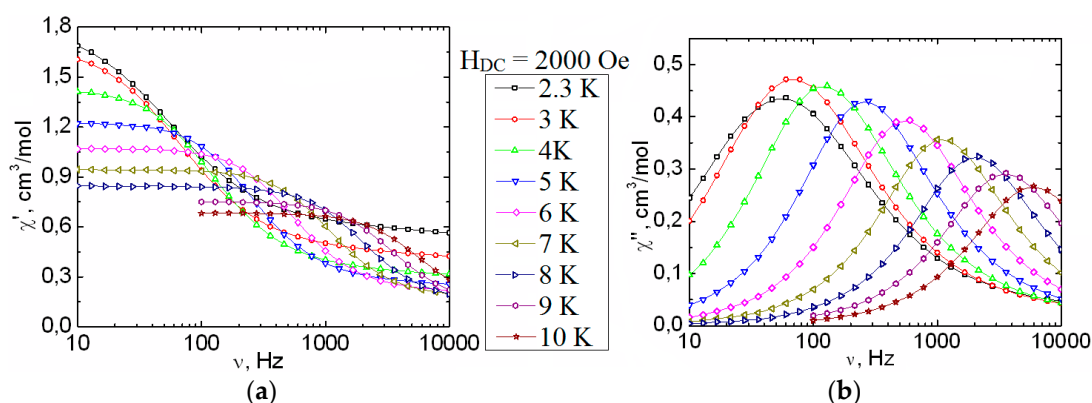


Figure 11. Frequency dependence of the in-phase (χ' , a) and out-of-phase (χ'' , b) parts of ac susceptibility, between 2 and 10 K, for 6 in a 2000 Oe dc field. Solid lines are visual guides.

To give a fuller picture, we also present our data [24] for ferrocenylacetate $[\text{Dy}(\text{fca})_3(\text{bpy})] \cdot \text{MeC}_6\text{H}_5$ (7). The structure of 7 contains the $[\text{Dy}(\text{fca})_3(\text{bpy})]$ complex (Figure 6) and solvate molecules of MeC_6H_5 . Bpy...bpy stacking interactions bind complexes into centrosymmetric dimers. The solvate molecule of MeC_6H_5 that is arranged in rather a spacious cavity is not involved in stacking interactions. Detailed studies of dc and ac magnetic susceptibility were carried out. SMM properties were detected at temperatures up to 32 K. Most likely, owing to the electron-donating effect of ferrocenyl moieties [45,46], the complex has an extremely high magnetization reversal barrier, $\Delta_{\text{eff}}/k_B = 241$ K, which is a record value for lanthanide β -diketonates. This result illustrates the importance of the effect of the crystal field on the SMM properties of dysprosium complexes.

3. Experimental Section

3.1. Materials and Methods

The following commercial reagents and solvents were used for the syntheses: hydrated dysprosium salts $\text{Dy}(\text{NO}_3)_3 \cdot 5\text{H}_2\text{O}$, $\text{DyCl}_3 \cdot 6\text{H}_2\text{O}$ and acetylacetonate $\text{Dy}(\text{acac})_3 \cdot 3\text{H}_2\text{O}$, from Alfa Aesar (Heysham, Lancashire, UK), cymantrene from Aldrich (St. Louis, MO, USA), acetylferrocene (Alfa Aesar, 97%) and solvents (MeOH, DMSO, $\text{C}_6\text{H}_5\text{Me}$, CHCl_3 , $\text{C}_2\text{H}_5\text{OH}$) from Alfa Aesar. Cymantrenecarboxylic acid was synthesized according to a known procedure by the reaction of cymantrenyllithium obtained from *n*-butyllithium and cymantrene in THF at -45°C , with solid CO_2 [47]. Before use in the synthesis, cymantrenecarboxylic acid was sublimed in vacuo to remove traces of Mn^{2+} . Methanol was dehydrated before use by distillation over magnesium; toluene was successively distilled over P_2O_5 and sodium; DMSO was purified by freezing.

Magnetic susceptibility measurements were performed with the use of a Quantum Design magnetometer/susceptometer PPMS-9 (Quantum Design, San Diego, CA, USA). This instrument works between 1.8 and 350 K for dc applied fields ranging from -9 to 9 T. For ac susceptibility measurements, an oscillating ac field of 1 or 5 Oe with a frequency between 10 and 10,000 Hz was employed. Measurements were performed on polycrystalline samples sealed in polyethylene bags and covered with mineral oil in order to prevent field-induced torquing of the crystals. The magnetic data were corrected for the sample holder, mineral oil and diamagnetic contribution.

X-ray powder diffraction analysis was carried out on a Bruker D8 ADVANCE X-ray diffractometer ($\text{CuK}\alpha$, Ni-filter, LYNXEYE detector, reflection geometry) (Bruker, Karlsruhe, Germany).

Experimental data from single crystals were obtained on a Bruker SMART APEX2 diffractometer [48] (Table S1). Absorption for **3** and **4** was taken into account by a semiempirical method based on equivalents using SADABS software [49]. For Compound **3**, the model of the isostructural Tb complex was used [23]. The positions of hydrogen atoms were calculated from geometrical considerations and refined using the “riding” model. The structure of **4** was determined using a combination of the direct method and Fourier syntheses. The structures of **3** and **4** were refined by the full-matrix anisotropic-isotropic least squares method. All of the calculations were carried out using SHELXS-2014 and SHELXL-2014 software [50]. CCDC 1493047 and 1493048 contain the supplementary crystallographic data for Compounds **3** and **4**. These data can be obtained free of charge via <http://www.ccdc.cam.ac.uk/conts/retrieving.html> or from the Cambridge Crystallographic Data Centre, 12 Union Road, Cambridge CB2 1EZ, U.K.; fax: (+44) 1223-336-033; or e-mail: deposit@ccdc.cam.ac.uk.

3.2. Synthesis of Complexes 1–4

Dysprosium complexes $[\text{Dy}_2(\text{O}_2\text{CCym})_6(\text{DMSO})_4]$ (**1**), $[\text{Dy}_2(\text{O}_2\text{CCym})_4(\text{NO}_3)_2(\text{DMSO})_4]$ (**2**) and $[\text{Dy}(\text{O}_2\text{CCym})(\text{acac})_2(\text{H}_2\text{O})]_n$ (**5**) were synthesized using the procedures that we developed previously [18,22]. The complex $[\text{Dy}_2(\text{O}_2\text{CFc})_4(\text{NO}_3)_2(\text{DMSO})_4]$ (**3**) was prepared according to the procedure used for the synthesis of its Gd and Tb isostructural analogs [23]. The complex $[\text{Dy}_2(\text{O}_2\text{CFc})_6(\text{DMSO})_2(\text{H}_2\text{O})_2] \cdot 2\text{DMSO} \cdot 3\text{MePh}$ (**4**) was obtained according to the procedure reported previously for the complex $[\text{Gd}_2(\text{O}_2\text{CFc})_6(\text{DMSO})_2(\text{H}_2\text{O})_2] \cdot 2\text{DMSO} \cdot 2\text{CH}_2\text{Cl}_2$ [23], except that boiling toluene (25 mL) was used for the extraction of the substance, and the resulting solution was kept at 4°C for two days.

4. Conclusions

In summary, we have obtained new findings on the magnetism of the lanthanide complexes with stable organometallic ligands. The analysis of complementary data on exchange coupling in binuclear complexes of gadolinium with two bridging oxygen atoms has shown the validity of the correlation between $J_{\text{Gd-Gd}'}$ and the Gd...Gd distance that we suggested earlier.

Dynamic ac magnetic susceptibility measurements have shown that the presence of more than one dysprosium atom in a molecule adversely affects the molecular magnet properties, since, as a rule,

SMM properties in polynuclear SMM are demonstrated by each lanthanide atom rather than by the exchange coupled systems as in complexes of d-elements. A considerable drawback of polynuclear lanthanide complexes lies in the existence of dipole-dipole coupling that accelerates relaxation processes and in their tendency to quantum tunneling, which noticeably decreases the real relaxation times. Furthermore, SMM characteristics are considerably affected by changes in local molecular symmetry and even insignificant distortion of coordination geometry. It has been shown also that the increase of the coordination number weakens the SMM properties of similar Dy complexes.

Supplementary Materials: The following are available online at www.mdpi.com/2312-7481/2/4/38/s1. Table S1: Crystal data and structure refinement for **3**, **4**, Figure S1: Plots of χT vs. temperature for **1–4** (▼, ▲, ●, ■, 1 [18]; ▲, 2; ●, 3; ■, 4). The measurements were carried out in an external magnetic field $H = 5000$ Oe, Figure S2: Frequency dependences of the in-phase (χ' , a) and out-of-phase (χ'' , b) parts of the ac susceptibility, between 2 and 6 K, for $[\text{Dy}_2(\text{O}_2\text{CCym})_6(\text{DMSO})_4]$ (**1**) in the zero dc field (this study). Solid lines are visual guides, Figure S3: Frequency dependences of the in-phase (χ' , a) and out-of-phase (χ'' , b) parts of the ac susceptibility, at 2 K, for $[\text{Dy}_2(\text{O}_2\text{CCym})_6(\text{DMSO})_4]$ (**1**) in the zero, 1000 and 2000 Oe dc field (this study). Solid lines are visual guides, Figure S4: τ vs. T^{-1} plot for $[\text{Dy}_2(\text{O}_2\text{CCym})_4(\text{NO}_3)_2(\text{DMSO})_4]$ (**2**) in the zero magnetic field. The solid red line is the best fit to the Arrhenius law ($\tau_0 = 3.2 \cdot 10^{-9}$ s, $\Delta E/k_B = 53$ K) (this study), Figure S5: Frequency dependences of the in-phase (χ' , a) and out-of-phase (χ'' , b) parts of the ac susceptibility, between 4 and 5 K, for $[\text{Dy}_2(\text{O}_2\text{CCym})_4(\text{NO}_3)_2(\text{DMSO})_4]$ (**2**) in a 1000 Oe dc field (this study). Solid lines are visual guides, Figure S6: Frequency dependences of the in-phase (χ' , a) and out-of-phase (χ'' , b) parts of the ac susceptibility, between 2 and 4 K, for $[\text{Dy}_2(\text{O}_2\text{Cfc})_4(\text{NO}_3)_2(\text{DMSO})_4]$ (**3**) in the zero dc field (this study). Solid lines are visual guides, Figure S7: Frequency dependences of the in-phase (χ' , a) and out-of-phase (χ'' , b) parts of the ac susceptibility, between 2 and 24 K, for $[\text{Dy}_2(\text{O}_2\text{Cfc})_4(\text{NO}_3)_2(\text{DMSO})_4]$ (**3**) in a 5000 Oe dc field (this study). Solid lines are visual guides, Figure S8: Frequency dependences of the in-phase (χ' , a) and out-of-phase (χ'' , b) parts of the ac susceptibility, at 2 K, for $[\text{Dy}_2(\text{O}_2\text{Cfc})_4(\text{NO}_3)_2(\text{DMSO})_4]$ (**3**) in the zero, 500, 1000 and 1500 Oe dc field (this study). Solid lines are visual guides, Figure S9: Frequency dependences of the in-phase (χ' , a) and out-of-phase (χ'' , b) parts of the ac susceptibility, at 2 K, for $[\text{Dy}_2(\text{O}_2\text{Cfc})_6(\text{DMSO})_2(\text{H}_2\text{O})_2]$ (**4**) in the zero, 1000, 1500, 2000 and 2500 Oe dc-field (this study). Solid lines are visual guides, Figure S10: Frequency dependences of the in-phase (a) and out-of-phase (b) parts of the ac susceptibility of $[\text{Dy}(\eta^2\text{-O}_2\text{CCym})_2(\mu\text{-O}_2\text{CCym})_4\text{Dy}(\text{H}_2\text{O})_4]_n$ (**5**) ($H_{dc} = 0$ Oe) [21], Figure S11: Plot of $\ln(\tau)$ vs. $1/T$ $[\text{Dy}(\eta^2\text{-O}_2\text{CCym})_2(\mu\text{-O}_2\text{CCym})_4\text{Dy}(\text{H}_2\text{O})_4]_n$ (**5**) obtained from the frequency dependences of χ'' in the zero magnetic field [21], Figure S12: Cole-Cole dependence for $[\text{Dy}_2(\text{O}_2\text{CCym})_6(\text{H}_2\text{O})_4]_n$ (**5**) ($H_{DC} = 0$ Oe), Figure S13: Frequency dependences of the in-phase (a) and out-of-phase (b) parts of the ac susceptibility of $[\text{Dy}(\text{CymCO}_2)(\text{acac})_2(\text{H}_2\text{O})]_n$ (**6**) ($H_{dc} = 0$ Oe) (this study), Figure S14: Frequency dependences of out-of-phase (χ'') parts of the ac susceptibility at 2.3 K, for $[\text{Dy}(\text{CymCO}_2)(\text{acac})_2(\text{H}_2\text{O})]_n$ (**6**) in the zero, 1000 and 2000 Oe dc field (this study). Solid lines are visual guides, Figure S15: τ vs. T^{-1} plot for $[\text{Dy}(\text{CymCO}_2)(\text{acac})_2(\text{H}_2\text{O})]_n$ (**6**) in a 2000 Oe dc field. The solid red line is the best fit to the Arrhenius law (this study).

Acknowledgments: This study was financially supported by the Russian Science Foundation (Grant 14-13-00938).

Author Contributions: P.S.K. and A.V.G. synthesized the complexes. N.N.E. and P.S.K. performed the experiments. A.B.I. performed the structural experiments. Z.V.D. conceived of and designed the experiments. Z.V.D., P.S.K. and N.N.E. wrote the paper. V.M.N. supervised and managed the project.

Conflicts of Interest: The authors declare no conflict of interest.

References

- Caneschi, A.; Gatteschi, R.; Sessoli, R.; Barra, A.L.; Brunel, L.C.; Guillot, M. Alternating current susceptibility, high field magnetization, and millimeter band EPR evidence for a ground $S = 10$ state in $[\text{Mn}_{12}\text{O}_{12}(\text{CH}_3\text{COO})_{16}(\text{H}_2\text{O})_4] \cdot 2\text{CH}_3\text{COOH} \cdot 4\text{H}_2\text{O}$. *J. Am. Chem. Soc.* **1991**, *113*, 5873–5874. [[CrossRef](#)]
- Sessoli, R.; Gatteschi, D.; Caneschi, A.; Novak, M.A. Magnetic bistability in a metal-ion cluster. *Nature* **1993**, *365*, 141–142. [[CrossRef](#)]
- Sessoli, R.; Powell, A.K. Strategies towards single molecule magnets based on lanthanide ions. *Coord. Chem. Rev.* **2009**, *253*, 2328–2341. [[CrossRef](#)]
- Bünzli, J.-C.G. Lanthanide coordination chemistry: From old concepts to coordination polymers. *J. Coord. Chem.* **2014**, *67*, 3706–3733. [[CrossRef](#)]
- Castro, G.; Regueiro-Figueroa, M.; Esteban-Gomez, D.; Perez-Lourido, P.; Platas-Iglesias, C.; Valencia, L. Magnetic anisotropies in rhombic lanthanide(III) complexes do not conform to bleaney's theory. *Inorg. Chem.* **2016**, *55*, 3490–3497. [[CrossRef](#)] [[PubMed](#)]

6. Gregson, M.; Chilton, N.F.; Ariciu, A.-M.; Tuna, F.; Crowe, I.F.; Lewis, W.; Blake, A.J.; Collison, D.; McInnes, E.J.L.; Winpenny, R.E.P.; et al. A Monometallic Lanthanide Bis(methanediide) Single molecule magnet with a large energy barrier and complex spin relaxation behaviour. *Chem. Sci.* **2016**, *7*, 155–165. [[CrossRef](#)]
7. Pointillart, F.; Guizouarn, T.; Lefevre, S.; Golhen, S.; Cador, O.; Ouahab, L. Rational design of a lanthanide-based complex featuring Different single-molecule magnets. *Chem. Eur. J.* **2015**, *21*, 16929–16934. [[CrossRef](#)] [[PubMed](#)]
8. Anastasiadis, N.C.; Kalofolias, D.A.; Philippidis, A.; Tzani, S.; Raptopoulou, C.P.; Psycharis, V.; Milios, C.J.; Escuer, A.; Perlepes, S.P. A family of dinuclear lanthanide(III) complexes from the use of a tridentate Schiff base: Structural and physical studies, and the case of a DyIII₂ emissive single-molecule magnet. *Dalton Trans.* **2015**, *44*, 10200–10209. [[CrossRef](#)] [[PubMed](#)]
9. Yattoo, M.A.; Cosquer, G.; Morimoto, M.; Irie, M.; Breedlove, B.K.; Yamashita, M. 1D chains of lanthanoid ions and a dithienylethene ligand showing slow relaxation of the magnetization. *Magnetochemistry* **2016**, *2*, 21–28. [[CrossRef](#)]
10. Huang, C. *Rare Earth Coordination Chemistry: Fundamentals and Applications*; John Wiley & Sons: Singapore, 2010.
11. Woodruff, D.N.; Winpenny, R.E.P.; Layfield, R.A. Lanthanide Single-Molecule Magnets. *Chem. Rev.* **2013**, *113*, 5110–5148. [[CrossRef](#)] [[PubMed](#)]
12. Chilton, N.F.; Langley, S.K.; Moubaraki, B.; Soncini, A.; Batten, S.R.; Murray, K.S. Single molecule magnetism in a family of mononuclear β -diketonate lanthanide(III) complexes: Rationalization of magnetic anisotropy in complexes of low symmetry. *Chem. Sci.* **2013**, *4*, 1719–1730. [[CrossRef](#)]
13. Mereacre, V.; Schlageter, M.; Powell, A.K. A temperature induced ferrocene-ferrocenium interconversion in a ferrocene functionalized μ_3 -O chromium carboxylate. *J. Magn. Magn. Mater.* **2015**, *381*, 478–480. [[CrossRef](#)]
14. Mereacre, V.; Schlageter, M.; Eichhöfer, A.; Bauer, T.; Wolny, J.A.; Schünemann, V.; Powell, A.K. Unusual metal-ligand charge transfer in ferrocene functionalized μ_3 -O iron carboxylates observed with Mössbauer spectroscopy. *J. Magn. Magn. Mater.* **2016**, *407*, 87–91. [[CrossRef](#)]
15. Koroteev, P.S.; Kiskin, M.A.; Dobrokhotova, Z.V.; Bogomyakov, A.M.; Efimov, N.N.; Novotortsev, V.M. Synthesis, structure, solid-state thermal decomposition and magnetic properties of binuclear Nd, Gd and Eu cymantrenecarboxylates. *Polyhedron* **2011**, *30*, 2523–2529. [[CrossRef](#)]
16. Koroteev, P.S.; Dobrokhotova, Z.V.; Kiskin, M.A.; Lermontov, A.S.; Efimov, N.N.; Bogomyakov, A.S.; Tyurin, A.V.; Bykov, M.A.; Demina, L.I.; Velikodny, Y.A.; et al. Synthesis, structure, thermal behavior, thermodynamic, magnetic and luminescent properties of Pr, Sm, Eu, and Gd cymantrenecarboxylates. *Polyhedron* **2012**, *43*, 36–46. [[CrossRef](#)]
17. Koroteev, P.S.; Dobrokhotova, Z.V.; Ilyukhin, A.B.; Motornova, M.S.; Novotortsev, V.M. Synthesis, structure, solid-state thermolysis, and catalytic properties of binuclear Ce, Nd, Eu, and Gd cymantrenecarboxylate complexes with DMSO. *Russ. Chem. Bull.* **2012**, *61*, 1069–1078. [[CrossRef](#)]
18. Koroteev, P.S.; Efimov, N.N.; Dobrokhotova, Z.V.; Ilyukhin, A.B.; Gavrikov, A.V.; Novotortsev, V.M. Binuclear and polynuclear cymantrenecarboxylate complexes of heavy lanthanides. *Russ. J. Coord. Chem.* **2015**, *41*, 149–161. [[CrossRef](#)]
19. Koroteev, P.S.; Dobrokhotova, Z.V.; Ilyukhin, A.B.; Efimov, N.N.; Kirdyankin, D.I.; Tyurin, A.V.; Velikodny, A.Y.; Kovba, M.L.; Novotortsev, V.M. Lanthanide cymantrenecarboxylate complexes with an Ln:Mn ratio of 1:2 as precursors for LnMn₂O₅ phases. Synthesis, structure, physicochemical properties, and thermal decomposition. *Polyhedron* **2013**, *65*, 110–121. [[CrossRef](#)]
20. Koroteev, P.S.; Dobrokhotova, Z.V.; Ilyukhin, A.B.; Efimov, N.N.; Kirdyankin, D.I.; Tyurin, A.V.; Gavrikov, A.V.; Novotortsev, V.M. Polymeric lanthanide acetates with peripheral cymantrenecarboxylate groups—Synthesis, magnetism and thermolysis. *Polyhedron* **2015**, *85*, 941–952. [[CrossRef](#)]
21. Koroteev, P.S.; Dobrokhotova, Z.V.; Ilyukhin, A.B.; Efimov, N.N.; Gavrikov, A.V.; Novotortsev, V.M. Polymer lanthanide cymantrenecarboxylates. *Russ. J. Coord. Chem.* **2015**, *41*, 805–816. [[CrossRef](#)]
22. Gavrikov, A.V.; Koroteev, P.S.; Dobrokhotova, Z.V.; Ilyukhin, A.B.; Efimov, N.N.; Kirdyankin, D.I.; Bykov, M.A.; Ryumin, M.A.; Novotortsev, V.M. Novel heterometallic polymeric lanthanide acetylacetonates with bridging cymantrenecarboxylate groups—Synthesis, magnetism and thermolysis. *Polyhedron* **2015**, *102*, 48–59. [[CrossRef](#)]

23. Koroteev, P.S.; Dobrokhotova, Z.V.; Efimov, N.N.; Ilyukhin, A.B.; Novotortsev, V.M. New binuclear ferrocenecarboxylates of rare-earth metals as precursors for ferrites: Syntheses, structures, and solid-phase thermolysis. *Russ. J. Coord. Chem.* **2014**, *40*, 495–504. [[CrossRef](#)]
24. Koroteev, P.S.; Dobrokhotova, Z.V.; Ilyukhin, A.B.; Efimov, N.N.; Rouzieres, M.; Kiskin, M.; Clerac, R.; Novotortsev, V.M. Synthesis, structure, and physical properties of new rare earth ferrocenoylacetates. *Dalton Trans.* **2016**, *45*, 6405–6417. [[CrossRef](#)] [[PubMed](#)]
25. Koroteev, P.S.; Dobrokhotova, Z.V.; Ilyukhin, A.B.; Efimov, N.N.; Novotortsev, V.M. Synthesis, structure, and magnetic properties of lanthanide ferrocenoylacetates with nitrate and 2,2'-bipyridine ligands. *J. Coord. Chem.* **2016**, *69*, 2723–2735. [[CrossRef](#)]
26. Benelli, C.; Gatteschi, D. Magnetism of lanthanides in molecular materials with transition-metal ions and organic radicals. *Chem. Rev.* **2002**, *102*, 2369–2387. [[CrossRef](#)] [[PubMed](#)]
27. Kahn, O. *Molecular Magnetism*; Wiley-Blackwell: New York, NY, USA, 1993; p. 380.
28. Panagiotopoulos, A.; Zafiropoulos, T.F.; Perlepes, S.P.; Bakalbassis, E.; Masson-Ramade, I.; Kahn, O.; Terzis, A.; Raptopoulou, C.P. Molecular structure and magnetic properties of acetato-bridged lanthanide(III) dimers. *Inorg. Chem.* **1995**, *34*, 4918–4920. [[CrossRef](#)]
29. Costes, J.P.; Clemente-Juan, J.M.; Dahan, F.; Nicodeme, F.; Verelst, M. Unprecedented Ferromagnetic Interaction in Homobinuclear Erbium and Gadolinium Complexes: Structural and Magnetic Studies. *Angew. Chem. Int. Ed.* **2002**, *41*, 323–325. [[CrossRef](#)]
30. Koroteev, P.S.; Efimov, N.N.; Dobrokhotova, Z.V.; Fomina, I.G.; Ilyukhin, A.B.; Eremenko, I.L.; Novotortsev, V.M. Magnetostructural correlation for the Gd complexes with bridging oxygen. *Russ. Chem. Bull. Int. Ed.* **2013**, *62*, 1768–1771. [[CrossRef](#)]
31. John, D.; Urland, W. Crystal Structure and Magnetic Behaviour of the New Gadolinium Carboxylates $Gd_2(CIF_2CCOO)_6(hypy)_2$, $Gd_2(F_3CCOO)_6(hypy)_2$, $Gd_2(F_2HCCOO)_6(hypy)_2$ and $Gd_2(Cl_2HCCOO)_6(H_2O)_2(hypy)_2$. *Eur. J. Inorg. Chem.* **2006**, 3503–3509. [[CrossRef](#)]
32. Roy, L.E.; Hughbanks, T. Magnetic Coupling in Dinuclear Gd Complexes. *J. Am. Chem. Soc.* **2006**, *128*, 568–575. [[CrossRef](#)] [[PubMed](#)]
33. Cañadillas-Delgado, L.; Fabelo, O.; Cano, J.; Pasán, J.; Delgado, F.S.; Lloret, F.; Julve, M.; Ruiz, C. Dinuclear and two- and three-dimensional gadolinium(III) complexes with mono- and dicarboxylate ligands: Synthesis, structure and magnetic properties. *CrystEngComm* **2009**, *11*, 2131–2142. [[CrossRef](#)]
34. Ito, M.; Hamada, D.; Ono, H.; Matsumoto, N.; Sunatsuki, Y.; Re, N. Binuclear tetra-acetate bridged Gd(III) complex $[Gd_2(\mu_2-O_2CMe)_4(H_2L)_2](ClO_4)_2 \cdot 2H_2O \cdot 2MeOH$ (H_2L = bis(5-methylimidazol-4-yl-methylideneamino propyl)methylamine): Synthesis, structure, and magnetic properties. *Inorg. Chim. Acta* **2016**, *443*, 274–278. [[CrossRef](#)]
35. Tumanski, S. *Handbook of Magnetic Measurements*; CRC Press, Taylor & Francis Group: Boca Raton, FL, USA, 2011; p. 62.
36. Bag, P.; Rastogi, C.K.; Biswas, S.; Sivakumar, S.; Mereacre, V.; Chandrasekhar, V. Homodinuclear lanthanide $\{Ln_2\}$ ($Ln = Gd, Tb, Dy, Eu$) complexes prepared from an o-vanillin based ligand: Luminescence and single-molecule magnetism behavior. *Dalton Trans.* **2015**, *44*, 4328–4340. [[CrossRef](#)] [[PubMed](#)]
37. Long, J.; Habib, F.; Lin, P.; Korobkov, I.; Enright, G.; Ungur, L.; Wernsdorfer, W.; Chibotaru, L.F.; Murugesu, M. Single-molecule magnet behavior for an antiferromagnetically superexchange-coupled dinuclear dysprosium(III) complex. *J. Am. Chem. Soc.* **2011**, *133*, 5319–5328. [[CrossRef](#)] [[PubMed](#)]
38. Sakamoto, S.; Fujinami, T.; Nishi, K.; Matsumoto, N.; Mochida, N.; Ishida, T.; Sunatsuki, Y.; Re, N. Carbonato-Bridged $Ni^{II}_2Ln^{III}_2$ ($Ln^{III} = Gd^{III}, Tb^{III}, Dy^{III}$) Complexes Generated by Atmospheric CO_2 Fixation and Their Single-Molecule-Magnet Behavior: $[(\mu_4-CO_3)_2\{Ni^{II}(3-MeOsaltN)(MeOH \text{ or } H_2O)Ln^{III}(NO_3)_2\}] \cdot solvent$ [3-MeOsaltN = N,N'-Bis(3-methoxy-2-oxybenzylidene)-1,3-propanediaminato]. *Inorg. Chem.* **2013**, *52*, 7218–7229. [[PubMed](#)]
39. Ehama, K.; Ohmichi, Y.; Sakamoto, S.; Fujinami, T.; Matsumoto, N.; Mochida, N.; Ishida, T.; Sunatsuki, Y.; Tsuchimoto, M.; Re, N. Synthesis, Structure, Luminescent, and Magnetic Properties of Carbonato-Bridged $Zn^{II}_2Ln^{III}_2$ Complexes $[(\mu_4-CO_3)_2\{Zn^{II}L^1Ln^{III}(NO_3)_2\}]$ ($Ln^{III} = Gd^{III}, Tb^{III}, Dy^{III}$; $L^1 = N,N'$ -Bis(3-methoxy-2-oxybenzylidene)-1,3-propanediaminato, $L^2 = N,N'$ -Bis(3-ethoxy-2-oxybenzylidene)-1,3-propanediaminato). *Inorg. Chem.* **2013**, *52*, 12828–12841. [[PubMed](#)]

40. Koroteev, P.S.; Ilyukhin, A.B.; Efimov, N.N.; Minin, V.V.; Tyurin, A.V.; Dobrokhotova, Z.V.; Novotortsev, V.M. Charge transfer adducts of binuclear rare earth 3,5-dinitrobenzoates with *N,N*-dimethylaniline and toluene. *Polyhedron* **2015**, *89*, 238–249. [[CrossRef](#)]
41. Katoh, K.; Horii, Y.; Yasuda, N.; Wernsdorfer, W.; Toriumi, K.; Breedlove, B.K.; Yamashita, M. Multiple-decker phthalocyaninato dinuclear lanthanoid(III) single-molecule magnets with dual-magnetic relaxation processes. *Dalton Trans.* **2012**, *41*, 13582–13600. [[CrossRef](#)] [[PubMed](#)]
42. Katoh, K.; Asano, R.; Miura, A.; Horii, Y.; Morita, T.; Breedlove, B.K.; Yamashita, M. Effect of f–f interactions on quantum tunnelling of the magnetization: Mono- and dinuclear Dy(III) phthalocyaninato triple-decker single-molecule magnets with the same octacoordination environment. *Dalton Trans.* **2014**, *43*, 7716–7725. [[CrossRef](#)] [[PubMed](#)]
43. Ungur, L.; Chibotaru, L.F. Strategies toward High-Temperature Lanthanide-Based Single-Molecule Magnets. *Inorg. Chem.* **2016**. [[CrossRef](#)] [[PubMed](#)]
44. Guo, Y.; Xu, G.; Gamez, P.; Zhao, L.; Lin, S.; Deng, R.; Tang, J.; Zhang, H. Two-step relaxation in a linear tetranuclear dysprosium(III) aggregate showing single-molecule magnet behavior. *J. Am. Chem. Soc.* **2010**, *132*, 8538–8539. [[CrossRef](#)] [[PubMed](#)]
45. McKinney, J.D.; Anderson, P.A.; Hamor, T.A.; Jones, C.J.; Paxton, K.; Porch, A. The synthesis, solid state conductivity and X-ray crystal structure of $[\text{Fe}(\eta^5\text{-C}_5\text{H}_5)(E\text{-}\eta^5\text{-C}_5\text{H}_4\text{-CH=CH-9-C}_{16}\text{H}_9)] [1,4\text{-}((\text{CN})_2\text{C}=\text{C})_2\text{C}_6\text{H}_4]$. *J. Organomet. Chem.* **1998**, *558*, 147–153. [[CrossRef](#)]
46. Perevalova, É.G.; Grandberg, K.I.; Zharikova, N.A.; Gubin, S.P.; Nesmeyanov, A.N. Electronic influence of ferrocenyl as a substituent. *Russ. Chem. Bull.* **1966**, *15*, 796–802. [[CrossRef](#)]
47. Nesmeyanov, A.N.; Anisimov, K.N.; Kolobova, N.E.; Makarov, Y.V. Metalation of cyclopentadienyltricarbonylmanganese. *Russ. Chem. Bull.* **1968**, *17*, 672. [[CrossRef](#)]
48. Bruker. *APEX2 and SAINT*; Bruker AXS Inc.: Madison, WI, USA, 2007.
49. Sheldrick, G.M. *SADABS*; University of Göttingen: Göttingen, Germany, 1997.
50. Sheldrick, G. Crystal structure refinement with SHELXL. *Acta Crystallogr. Sect. C* **2015**, *71*, 3–8. [[CrossRef](#)] [[PubMed](#)]



© 2016 by the authors; licensee MDPI, Basel, Switzerland. This article is an open access article distributed under the terms and conditions of the Creative Commons Attribution (CC-BY) license (<http://creativecommons.org/licenses/by/4.0/>).